



HAL
open science

Optimization of the measurement of residual stresses by the incremental hole drilling method. Part I: Numerical correction of experimental errors by a configurable numerical–experimental coupling

A.S. Ibrahim Mamane, S. Giljean, M.-J. Pac, G. L’hostis

► To cite this version:

A.S. Ibrahim Mamane, S. Giljean, M.-J. Pac, G. L’hostis. Optimization of the measurement of residual stresses by the incremental hole drilling method. Part I: Numerical correction of experimental errors by a configurable numerical–experimental coupling. *Composite Structures*, 2022, 294, pp.115703. 10.1016/j.compstruct.2022.115703 . hal-04044920

HAL Id: hal-04044920

<https://hal.science/hal-04044920>

Submitted on 24 Mar 2023

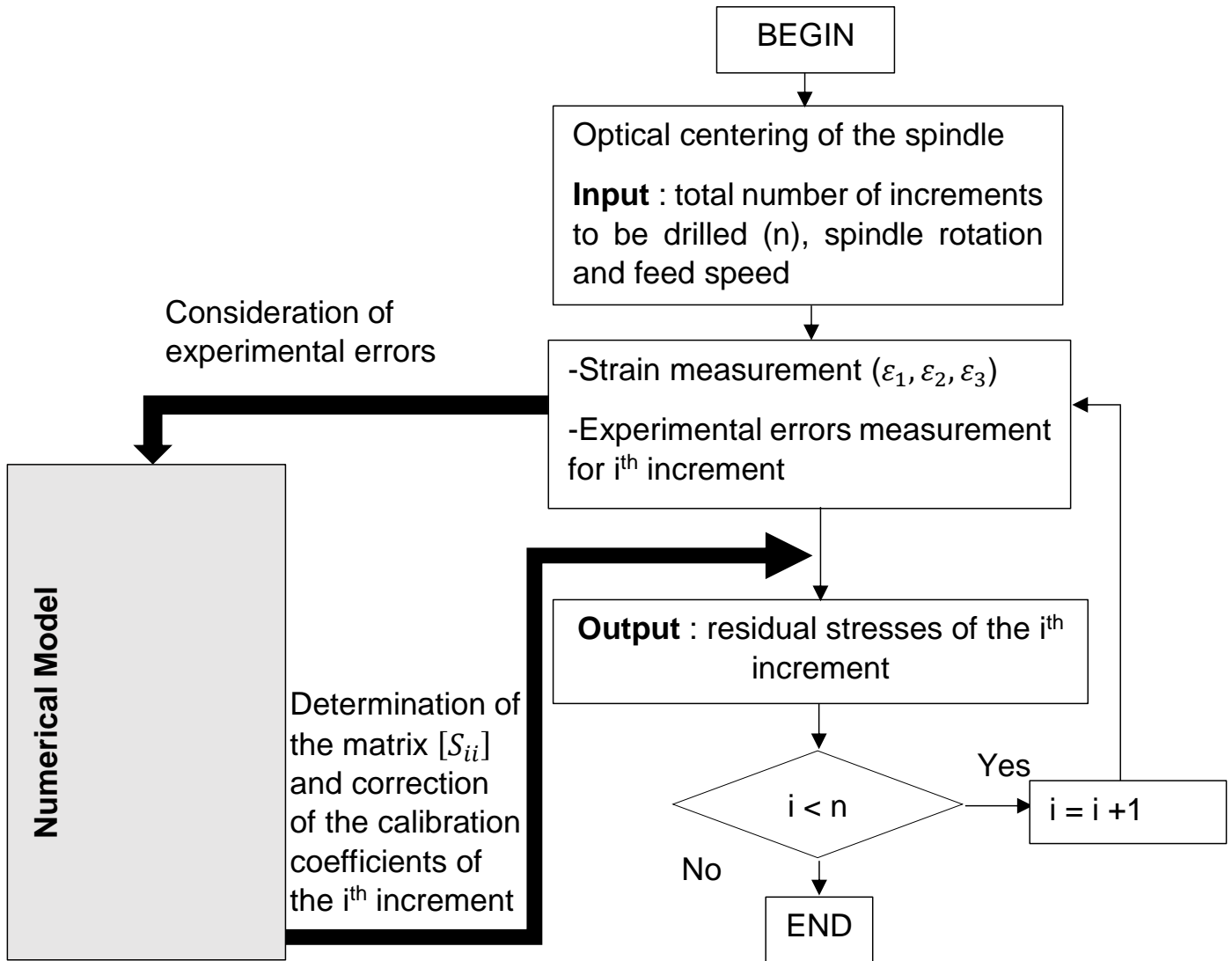
HAL is a multi-disciplinary open access archive for the deposit and dissemination of scientific research documents, whether they are published or not. The documents may come from teaching and research institutions in France or abroad, or from public or private research centers.

L’archive ouverte pluridisciplinaire **HAL**, est destinée au dépôt et à la diffusion de documents scientifiques de niveau recherche, publiés ou non, émanant des établissements d’enseignement et de recherche français ou étrangers, des laboratoires publics ou privés.

Graphical Abstract

Optimization of the measurement of residual stresses by the incremental hole drilling method. Part I: numerical correction of experimental errors by a configurable numerical-experimental coupling.

A.S. Ibrahim Mamane, S. Giljean, M.-J. Pac, G. L'Hostis



Optimization of the measurement of residual stresses by the incremental hole drilling method. Part I: numerical correction of experimental errors by a configurable numerical-experimental coupling.

A.S. Ibrahim Mamane*, S. Giljean, M.-J. Pac and G. L'Hostis

Université de Haute Alsace, Laboratoire de Physique et Mécanique Textiles (EA 4365), F-68093 Mulhouse, France

ARTICLE INFO

Keywords:

Fiber reinforced composites
Residual stresses
Experimental errors
Numerical correction

ABSTRACT

The incremental hole drilling method is very effective in measuring the residual stress gradient in composite laminates. However, its reliability depends on the accuracy with which the calibration coefficients are determined. These coefficients are calculated using a finite element model. The samples' features and the real experimental conditions must be taken into account in the simulation. Any mismatch can lead to inadequate calibration coefficients, thus introducing errors on residual stresses. Several calibration coefficients correction models exist for isotropic materials, but there is a lack of information on this subject concerning composite laminates. In this paper, the influence of three major experimental errors on the calibration coefficients is numerically investigated for composite laminates. The sensitivity of the coefficients to these errors is highlighted and a numerical correction method is proposed.

1. Introduction

Fiber reinforced composites are well known for their good specific properties [1], but they are particularly subject to residual stresses due to their heterogeneity. Residual stresses have different origins at different scales. On the micromechanical level, the mismatch in coefficient of thermal expansion between fibers and matrix causes non-uniform volumetric shrinkage during cooling [2, 3, 4]. On the ply-to-ply scale, the anisotropic thermal behavior of the layers depending on the orientation of the fibers causes constrained shrinkage [5]. Residual stresses also form at macroscopic level due to temperature gradient through composite thickness during cooling [6]. These multi-scale residual stresses influence the behavior of composite materials and can generate geometric distortions, fiber buckling, and composite damage in the form of micro-cracks and/or delamination [7]. This problem also affects recent manufacturing techniques based on layer-by-layer polymerization such as 3D printing.


There are many methods to measure residual stresses in composite laminates and much research is being done to improve them. Residual stresses can be measured by the curvature method [8, 9] adapted for thin unsymmetrical laminates. X-ray diffraction is a powerful method, which requires the insertion of crystalline particles between layers, but not easily performed [10]. Other methods exist like layer removal [11] which gives the profile of residual stresses layer by layer, compliance method [4] which measures relaxation strains from slits in the thickness and incremental hole drilling method [12]. Guo et al. [13] recently classified the main

methods of measuring residual stresses by specifying their advantages and limitations. The incremental hole drilling is one of the most widely used method because of its reliability, good accuracy, the availability of standard test procedure [14] and its ability to take into account the non-uniformity of residual stresses in the thickness without severely damaging the material.

The incremental hole drilling is a semi-destructive method which consists of drilling a step by step hole through the thickness of the material. For each increment, relaxation deformations around the hole are measured and calibration coefficients are calculated using a finite element model to evaluate the gradient of residual stresses in the material. This method is very sensitive to experimental errors. Any error in measuring, conditioning equations or experimental device design can lead to unreliable stress results. Several authors have studied the influence of these errors on the measurement of residual stresses in the case of isotropic materials. Schajer and Altus [15] have shown how to calculate the deviation of residual stresses with a given probability from the experimental errors. Ajovalasit [16] has proposed an analytical correction of the eccentricity of the hole for thin isotropic materials. More recently, Beghini et al. [17, 18] introduced the influence functions to analytically correct the eccentricity for blind hole in thick isotropic materials.

In this work, a configurable Python script is developed to generate the needed finite element models. The capability of the script to generate configurable models allowed to perform a parametric study and to assess the influence of experimental errors on the calibration coefficients for composite laminates. Among them, a focus is done on three main sources of errors : errors on increment depth, angular de-

*Corresponding author

 aboubakar-sedick.ibrahim-mamane@uha.fr (A.S.I. Mamane)

ORCID(s):

viation of the gages from their theoretical position and hole eccentricity errors. A detailed analysis of the results is presented in section 4. Beyond the automation of the tasks and the performance of parametric studies, the developed numerical tools allowed to introduce a novel correction method of the calibration coefficients. This numerical correction method is adapted for thick composite laminates for which the analytical approach is too complex. The method is formulated to correct any errors that can be experimentally measured and numerically modelled.

2. Historical evolution of the hole-drilling method

The hole drilling method was originally proposed by Josef Mathar [19] in 1933 for isotropic materials. Mathar used mechanical extensometer to measure deformations in the vicinity of the hole. This severely limited the accuracy and reliability of the method. In 1950, Soete and Vancrombrugge [20] introduced the use of strain gages in the application of the hole method. This improved the measurement of deformations around the hole. They also proposed an incremental approach that takes into account the non-uniformity of residual stresses in material thickness. In 1966, Rendler and Vigness [21] standardized the incremental hole method by adopting a precise geometry of the strain gages and defining calibration coefficients to link the relaxation deformations to the residual stresses. They showed that the residual stress calculation was repeatable. Their work later served as the basis for ASTM E837. Bert and Thomson [22] used a similar method to calculate the residual stresses in orthotropic materials.

In the incremental hole method so far used, residual stresses were considered uniform in a given increment regardless of the geometric variation of the hole. In 1978, Bijak-Zochowski [23] proposed a method called "integral method", which allows to take into account the variation of residual stresses in the same increment when the depth of the hole increases. This method was initially poorly exploited because of the complexity of experimentally determining calibration coefficients for each increment. In 1981, Schajer [24] showed that it was possible to use finite element simulations to reliably calculate calibration coefficients. He proposed the «power series method» which is an approximation of the integral method. With the evolution of finite element simulations, authors such as Niku-Lari et al. [25] and Flaman and Manning [26] have contributed to the improvement of the integral method. In 1994, Schajer and Yang [27] showed, unlike Bert and Thomson, that it was not possible to extend the equations of Rendler and Vigness to orthotropic materials. They proposed a new approach that takes into account the orthotropy of the material.

The first numerical models used to determine calibration coefficients [24] were axisymmetric models. In 2002, Aoh and Wei [28] used a 3D numerical model to calculate calibration coefficients. Among other things, they showed the influence of the thickness of the model on the values of the calibration

coefficients. They concluded that a 3D model was more representative of reality than an axisymmetric model. In 2003, Sicot et al [29] adapted Bert and Thomson's approach to the integral method and extended it to the calculation of residual stresses in laminated composites. In 2007, Shokrieh and Ghasemi [30] used the integral form of Schajer and Yang's approach, to determine residual stresses in laminated composites. More recently, in 2016, Ghasemi and Mohammadi [31] used the same method to determine residual stresses in fiber-metal laminates. The incremental hole method continues to be the subject of several researches which make it increasingly optimal. Barsanti et al. [32] proposed a solution to counter the effect of hole eccentricity for isotropic materials, Blödorn et al. [33] studied the effect of hole bottom geometry on residual stresses. In 2020, Schajer [34] introduced a compact form of the calibration data to facilitate their use and reduce computation time.

3. Calculation of the calibration coefficients

The incremental hole drilling method consists in drilling a hole incrementally through the thickness of a material. The strains around the hole are measured for each increment using three gages. These strains, which are measured on the surface of the material, are the sum of the strains due to all the increments. This is given by the following equation [35]:

$$\epsilon_k^i = \sum_{l=1}^3 \sum_{j=1}^i (C_{ijkl} \sigma_l^j) \quad (1)$$

Where $0 < k \leq 3$ and $0 < l \leq 3$.

ϵ_k^i : is the strain given by gage "k" when the depth of the hole corresponds to "i" increments

σ_l^j : are the residual stresses. "l" represents the stress components ($\sigma_1 = \sigma_x$, $\sigma_2 = \sigma_{xy}$ and $\sigma_3 = \sigma_y$)

C_{ijkl} : is the matrix of calibration coefficients related to the increment "j" when the total number of increments is "i".

This equation can be written in matrix form:

$$\{\epsilon\} = [C] \{\sigma\} \quad (2)$$

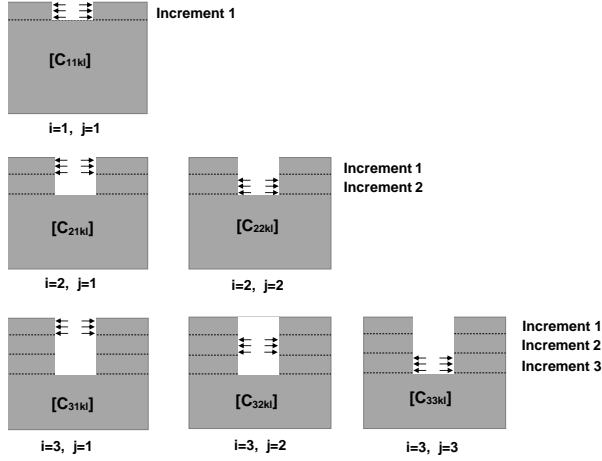
The expansion of Eq. 2 for three increments is presented in Fig. 1a.

The number of necessary coefficients increases rapidly with the increments. For 3 increments, 54 coefficients are needed (Fig. 1a). For isotropic materials, Schajer, recently, proposed a compact form for calibration data with only 15 numerical coefficients to be determined [34]. Such work for anisotropic cases would reduce computation time and facilitate the use of calibration data.

To calculate residual stresses, the exact values of the calibration coefficients must be determined. These coefficients depend on the radius of the hole and the geometry of the

$$\begin{pmatrix} \epsilon_1^1 \\ \epsilon_2^1 \\ \epsilon_3^1 \\ \epsilon_1^2 \\ \epsilon_2^2 \\ \epsilon_3^2 \\ \epsilon_1^3 \\ \epsilon_2^3 \\ \epsilon_3^3 \end{pmatrix} = \begin{bmatrix} C_{1111} & C_{1112} & C_{1113} & 0 & 0 & 0 \\ C_{1121} & C_{1122} & C_{1123} & 0 & 0 & 0 \\ C_{1131} & C_{1132} & C_{1133} & 0 & 0 & 0 \\ C_{2111} & C_{2112} & C_{2113} & C_{2211} & C_{2212} & C_{2213} \\ C_{2121} & C_{2122} & C_{2123} & C_{2221} & C_{2222} & C_{2223} \\ C_{2131} & C_{2132} & C_{2133} & C_{2231} & C_{2232} & C_{2233} \\ C_{3111} & C_{3112} & C_{3113} & C_{3211} & C_{3212} & C_{3213} \\ C_{3121} & C_{3122} & C_{3123} & C_{3221} & C_{3222} & C_{3223} \\ C_{3131} & C_{3132} & C_{3133} & C_{3231} & C_{3232} & C_{3233} \end{bmatrix} \begin{pmatrix} \sigma_x^1 \\ \sigma_{xy}^1 \\ \sigma_y^1 \\ \sigma_x^2 \\ \sigma_{xy}^2 \\ \sigma_y^2 \\ \sigma_x^3 \\ \sigma_{xy}^3 \\ \sigma_y^3 \end{pmatrix}$$

(a)



(b)

Figure 1: (a) Expansion of the relation between residual stresses and relaxation strains for three increments, (b) Load cases to calculate the different matrices of calibration coefficients

gages used. To determine the coefficients, a known numerical stress field is applied to the material (Fig. 1b) and the relaxation strains around the hole are calculated. The computation is done using a finite element model.

For increment 1:

$$\epsilon_k^1 = C_{11kl} \sigma_l^1 \quad (3)$$

The three deformations ϵ_k^1 are experimentally measured and C_{11kl} are numerically calculated. σ_l^1 can, therefore, be determined.

For increment 2:

$$\epsilon_k^2 = C_{21kl} \sigma_l^1 + C_{22kl} \sigma_l^2 \quad (4)$$

$C_{21kl} \sigma_l^1$ and $C_{22kl} \sigma_l^2$ are respectively the contribution of the residual stresses of the first and second increments to the total strain measured at the surface ϵ_k^2 . Here, σ_l^2 can be calculated. In the same way, the gradient of residual stresses in the material is determined increment by increment up to the limit depth of sensitivity of the gages.

Application 1:

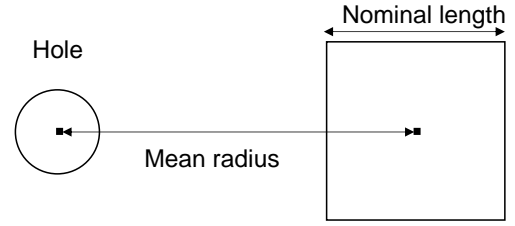


Figure 2: Definition of the mean radius and the nominal length of the strain gage rosette modelled as strain extraction areas in the numerical simulation

In this application, the different steps to calculate the calibration coefficients of a $[0_2/90_2]_s$ carbon/epoxy composite laminates are detailed. The material is modelled in 3D using the commercial finite element software ABAQUS. Each layer has a thickness of 0.2 mm. EA-06-062RE-120 strain gages, designed by Micro-Measurements, are modelled as strain measuring areas. The mean radius of the strain-gage rosette is $r_m = 2.57$ mm and its nominal length is 1.59 mm (Fig. 2). 2 increments per ply are simulated. The radius of the hole is 1 mm and the material properties are given in Table 1.

For a given increment, the calibration coefficients are calculated from Eq. 5 using 3 different load cases:

$$\frac{1}{\sqrt{E_x E_y}} \begin{bmatrix} c_{ij11} & c_{ij12} & c_{ij13} \\ c_{ij21} & c_{ij22} & c_{ij23} \\ c_{ij31} & c_{ij32} & c_{ij33} \end{bmatrix} \begin{Bmatrix} \sigma_x^i \\ \sigma_{xy}^i \\ \sigma_y^i \end{Bmatrix} = \begin{Bmatrix} \epsilon_1^i \\ \epsilon_2^i \\ \epsilon_3^i \end{Bmatrix} \quad (5)$$

$$c_{ijkl} = C_{ijkl} \sqrt{E_x E_y}$$

E_x and E_y are Young's moduli following the main directions of the composite.

Load 1: longitudinal uni-axial tensile stress to determine c_{ij11} , c_{ij21} and c_{ij31} (Fig. 3a):

$$\frac{1}{\sqrt{E_x E_y}} \begin{bmatrix} c_{ij11} & c_{ij12} & c_{ij13} \\ c_{ij21} & c_{ij22} & c_{ij23} \\ c_{ij31} & c_{ij32} & c_{ij33} \end{bmatrix} \begin{Bmatrix} \sigma_x^i \\ 0 \\ 0 \end{Bmatrix} = \begin{Bmatrix} \epsilon_1^i \\ \epsilon_2^i \\ \epsilon_3^i \end{Bmatrix} \quad (6)$$

Load 2: transverse uni-axial tensile stress to determine c_{ij13} , c_{ij23} and c_{ij33} (Fig. 3b):

$$\frac{1}{\sqrt{E_x E_y}} \begin{bmatrix} c_{ij11} & c_{ij12} & c_{ij13} \\ c_{ij21} & c_{ij22} & c_{ij23} \\ c_{ij31} & c_{ij32} & c_{ij33} \end{bmatrix} \begin{Bmatrix} 0 \\ 0 \\ \sigma_y^i \end{Bmatrix} = \begin{Bmatrix} \epsilon_1^i \\ \epsilon_2^i \\ \epsilon_3^i \end{Bmatrix} \quad (7)$$

Load 3: shear stress to determine c_{ij12} , c_{ij22} and c_{ij32}

Table 1

Mechanical properties of the carbon/epoxy used in the numerical simulations [36]

$E_1(MPa)$	$E_2(MPa)$	$E_3(MPa)$	$G_{12}(MPa)$	$G_{13}(MPa)$	$G_{23}(MPa)$	ν_{12}	ν_{13}	ν_{23}
229000.00	12000.00	12000.00	5140.00	5140.00	4080.00	0.32	0.32	0.49

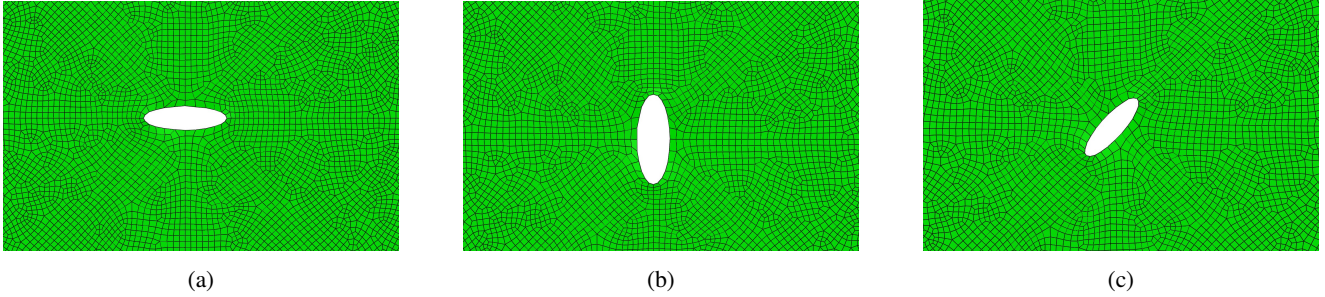


Figure 3: Material deformations associated with the 3 load cases (through-the-thickness hole in this illustration): (a) deformation associated with the longitudinal uni-axial tensile stress, (b) deformation associated with the transverse uni-axial tensile stress and (c) deformation associated with the shear stress

(Fig. 3c):

$$\frac{1}{\sqrt{E_x E_y}} \begin{bmatrix} c_{ij11} & c_{ij12} & c_{ij13} \\ c_{ij21} & c_{ij22} & c_{ij23} \\ c_{ij31} & c_{ij32} & c_{ij33} \end{bmatrix} \begin{Bmatrix} 0 \\ \sigma_{xy}^i \\ 0 \end{Bmatrix} = \begin{Bmatrix} \epsilon_1^i \\ \epsilon_2^i \\ \epsilon_3^i \end{Bmatrix} \quad (8)$$

When an increment "i" is numerically drilled (removal of elements), the 3 load cases are successively applied to the different increments j , $0 \leq j \leq i$. For example, to calculate the matrix $[c_{32kl}]$, the loads must be applied to the second increment ($j=2$) when $i=3$, see Fig. 1b. If gage 1 is oriented in on-axis direction of the first layer then c_{ij12} and c_{ij32} are always equal to zero.

The three loads are applied on the wall of the hole. A change from Cartesian coordinate system to cylindrical is therefore necessary.

$$\begin{cases} \sigma_{rr} = \sigma_x (\cos \theta)^2 + \sigma_y (\sin \theta)^2 + \sigma_{xy} \sin(2\theta) \\ \sigma_{\theta r} = \frac{\sigma_y - \sigma_x}{2} \sin(2\theta) + \sigma_{xy} \cos(2\theta) \end{cases} \quad (9)$$

Load 1: $\sigma_x = \sigma; \sigma_y = \sigma_{xy} = 0$

$$\begin{cases} \sigma_{rr} = \sigma (\cos \theta)^2 \\ \sigma_{\theta r} = -\sigma \sin(\theta) \cos(\theta) \end{cases} \quad (10)$$

Load 2: $\sigma_y = \sigma; \sigma_x = \sigma_{xy} = 0$

$$\begin{cases} \sigma_{rr} = \sigma (\sin \theta)^2 \\ \sigma_{\theta r} = \sigma \sin(\theta) \cos(\theta) \end{cases} \quad (11)$$

Load 3: $\sigma_{xy} = \sigma; \sigma_x = \sigma_y = 0$

$$\begin{cases} \sigma_{rr} = \sigma \sin(2\theta) \\ \sigma_{\theta r} = \sigma \cos(2\theta) \end{cases} \quad (12)$$

Meshing is a key step of the simulation. The better the mesh, the more accurate the results. The model is meshed with 8-node linear brick isoparametric elements (C3D8R). The mesh is configured in such a way as to guarantee its quality whatever the geometric parameters. To have the most uniform mesh, the model is partitioned along its diagonals and its two axes of symmetry. The elements sizes depend on the geometric parameters of the model. In addition, a circular partition around the hole delimits an area of interest where the mesh is refined (Fig. 4a). In the thickness, the elements size is defined by the choice of the number of elements per increment (Fig. 4b).

Gage 1 is oriented at 0 degrees, gage 2 at 225 degrees and gage 3 at 90 degrees with respect to the on-axis direction of the first layer (Fig. 4a). For the first increment, one obtains:

$$[c_{11kl}] = \begin{bmatrix} -0.0291 & 0 & 0.0008 \\ -0.0106 & -0.0713 & -0.0268 \\ -0.0014 & 0 & -0.0545 \end{bmatrix} \quad (13)$$

4. Numerical investigation on the most influential experimental errors

The incremental hole drilling method must be performed with great care to have reliable results. The experimental errors can be divided into 2 categories, according to their sources. Category 1 concerns strain measurement errors which may occur due to additional thermal strains, instrument calibration errors, additional residual stresses caused by hole drilling [15]. These errors affect the left side of Eq. 2. They are independent of the initial state of residual stresses within

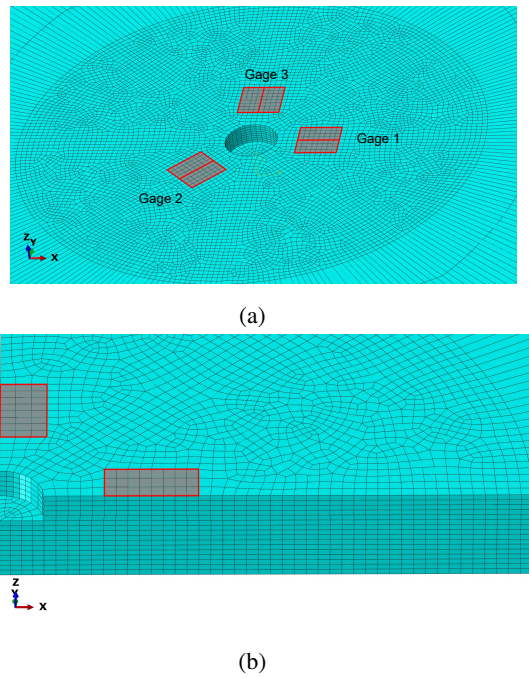


Figure 4: Mesh strategy using 8-node linear brick isoparametric elements: (a) Mesh refinement area, gage 1 is oriented in the direction of the fibers which corresponds to the x-axis, (b) Structured mesh in the thickness, the number of elements per increment is configurable

the material and their effect is additive. The category 1 errors are difficult to assess and to correct. Category 2 (category 2-5 type errors of reference [15]) concerns errors in the experimental parameters such as errors on increment depth, misalignment of the gages with respect to the fibers, hole eccentricity errors, hole diameter measurement errors. The effects of these errors are proportional to the initial state of residual stresses (Eq. 2). For example, if a material without residual stresses is considered, whatever the errors on the increment depth no additional residual stresses will be measured. The category 2 errors affect the right side of Eq. 2 and they can be measured and corrected. The overall errors on the measured residual stresses are the sum of the category 1 and category 2 errors. This paper focuses on the study of category 2 errors.

The residual stresses errors caused by category 2 errors are due to the mismatches between the numerical simulation and the experimental procedure of the incremental hole drilling method. In general, there are three scenarios. These scenarios apply to all category 2 errors, but, for the sake of understanding, they are detailed below using the example of errors on increment depth (Fig. 5a).

- Scenario 1:
The residual stresses are determined using the calibration coefficients calculated for the desired experimental parameters (d_{model} , Fig. 5a) and the relaxation strains measured for the desired experimental parameters (d_{model}). There is no mismatch between the ex-

perimentation and the numerical simulation \Rightarrow ideal experimental device.

- Scenario 2:
The residual stresses are determined using the calibration coefficients calculated for the desired experimental parameters (d_{model}) and the relaxation strains measured for the real experimental parameters (d_{exp}). There is a mismatch between the experimentation and the numerical simulation \Rightarrow standard error.
- Scenario 3:
The calibration coefficients are corrected by taking into account the experimental errors in the simulation. The residual stresses are determined using the corrected calibration coefficients (d_{exp}) and the relaxation strains measured for the real experimental parameters (d_{exp}). There is no more mismatch between the experimentation and the simulation \Rightarrow numerical correction of the calibration coefficients.

In practice, Scenario 2 is always carried out. Scenario 3 is detailed in section 5.

4.1. Development of a configurable numerical model

Program scripts are commonly used to automate the post-processing of incremental hole drilling simulation results. Here, in addition to post-processing, the modeling and simulation steps are also automated using a Python script. This script is configured to create different sample sizes, different material properties, different types of gages, different types of stratifications, different drilling strategies, different types of meshes, different load cases depending on the input data. The Python program is used with the commercial finite element software ABAQUS. Once all the input data are provided and the program is executed, it performs the following tasks: creation of the model on ABAQUS, simulation of the incremental hole drilling, extraction of the output data, namely the radial strains, in the areas corresponding to the gages and finally calculation and storage of the calibration coefficients in a file (Fig. 6). The configurable aspect of the developed model allowed to perform a numerical investigation to assess the sensitivity of the calibration coefficients to the main sources of category 2 errors : error on increment depth, angular deviation of the gages from their theoretical position and hole eccentricity errors (Fig. 5). The correction method presented in section 5 is also based on the developed configurable numerical model.

4.2. Errors on increment depth

Inaccuracies in the depth of increments are generally caused by the positioning uncertainties of the motor driving the spindle advance and by geometric defects of the experimental device. Due to these inaccuracies, the drilled increment depth

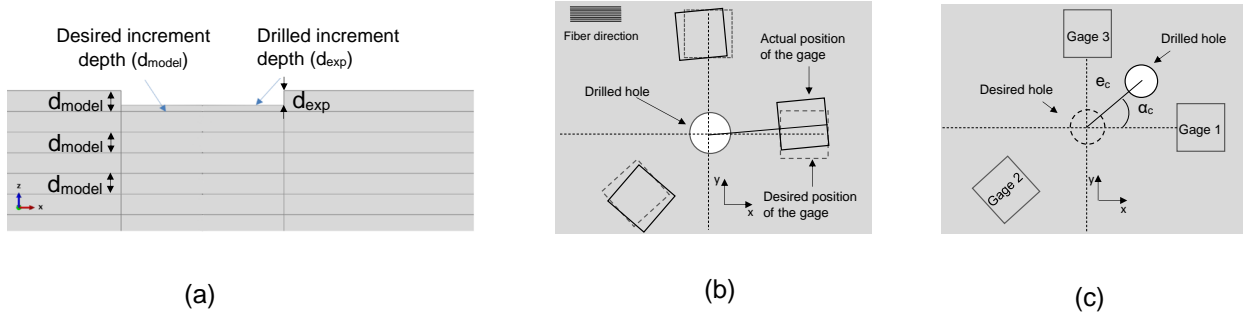


Figure 5: Presentation of the studied errors: (a) errors on increment depth, (b) Angular deviation of the gages from their theoretical position, (c) Radial (e_c) and angular (α_c) eccentricity of the hole

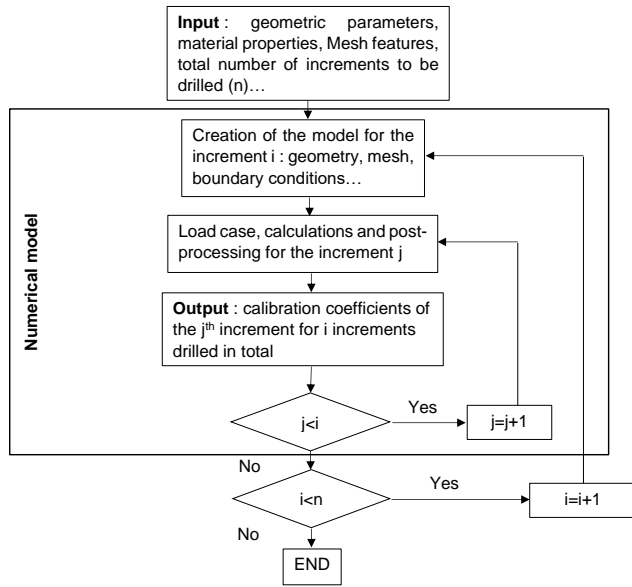


Figure 6: The different steps of the configurable numerical model developed for the custom calculation of calibration coefficients and the execution of parametric studies

d_{exp} is different from the desired increment depth d_{model} (Fig. 5a). This is one of the main sources of error when measuring residual stresses.

$$d_{exp} = d_{model} \pm \delta d_{model} \quad (14)$$

Where δd_{model} is the error on increment depth.

All calibration coefficients c_{ijkl} are calculated for the desired increment depth d_{model} . To determine the correct residual stresses, relaxation strains must be experimentally measured for the exact same increment depth. However, the experimentally measured strains correspond to the drilled increment depths (d_{exp}). This leads to errors in the calculation of residual stresses (Scenario 2).

From Eq. 5, one can write:

$$\sigma_x^i = (k_1 \epsilon_1^i + k_2 \epsilon_3^i) \sqrt{E_x E_y} \quad (15)$$

$$\sigma_y^i = (k_3 \epsilon_1^i + k_4 \epsilon_3^i) \sqrt{E_x E_y} \quad (16)$$

$$\sigma_{xy}^i = (k_5 \epsilon_1^i + k_6 \epsilon_2^i + k_7 \epsilon_3^i) \sqrt{E_x E_y} \quad (17)$$

The expressions of all the coefficients k_p , $1 \leq p \leq 16$, and K_p , $1 \leq p \leq 15$, are given in the appendix.

Considering category 2 errors, the non-correction of the calibration coefficients leads to errors on the residual stresses given by:

$$\delta \sigma_x^i = (K_1 \epsilon_1^i + K_2 \epsilon_3^i) \sqrt{E_x E_y} \quad (18)$$

$$\delta \sigma_y^i = (K_3 \epsilon_1^i + K_4 \epsilon_3^i) \sqrt{E_x E_y} \quad (19)$$

$$\delta \sigma_{xy}^i = (K_5 \epsilon_1^i + K_6 \epsilon_3^i) \sqrt{E_x E_y} \quad (20)$$

Depth perturbations δd_{model} are introduced in the numerical model in order to study the variations of the coefficients c_{ijkl} . The results are presented in the form of a table which gives the value of the calibration coefficients for the different errors on increment depth (Table 2) and in the form of 2 graphs, one giving the variation of the calibration coefficients in percentage (Fig. 7a) and the other giving the variation of the coefficients K_p , $1 \leq p \leq 6$, of Eq.18-20 (Fig. 7b).

For the different depth perturbations δd_{model} , the coefficients have the same direction of variation. If δd_{model} is positive, the absolute values of the coefficients increase and if it is negative, their absolute values decrease. The variation of all the coefficients is quasi-linear, they are proportional to the relaxation strains (Eq. 6-8). As seen in Eq. 1, the relaxation strains depend on the increment depth, so, if d_{exp} is greater than d_{model} , the strains are overestimated and if d_{exp} is less than d_{model} , they are underestimated. The influence on residual stresses is more directly reflected by the varia-

Table 2

variation of the calibration coefficients c_{11kl} for different errors on increment depth δd_{model} (increment depth $d_{model} = 100\mu m$).

$\delta d_{model}/d_{model}$	c_{1111}	c_{1121}	c_{1131}	c_{1122}	c_{1113}	c_{1123}	c_{1133}
0	-0.0291	-0.0106	-0.0014	-0.0713	0.0008	-0.0268	-0.0545
-10%	-0.0265	-0.0095	-0.0013	-0.0641	0.0006	-0.0236	-0.0508
+10%	-0.0326	-0.0120	-0.0015	-0.0793	0.0011	-0.0287	-0.0614
+25%	-0.0385	-0.0147	-0.0016	-0.0925	0.0014	-0.0340	-0.0693
+50%	-0.0485	-0.0181	-0.0017	-0.1107	0.0019	-0.0400	-0.0854

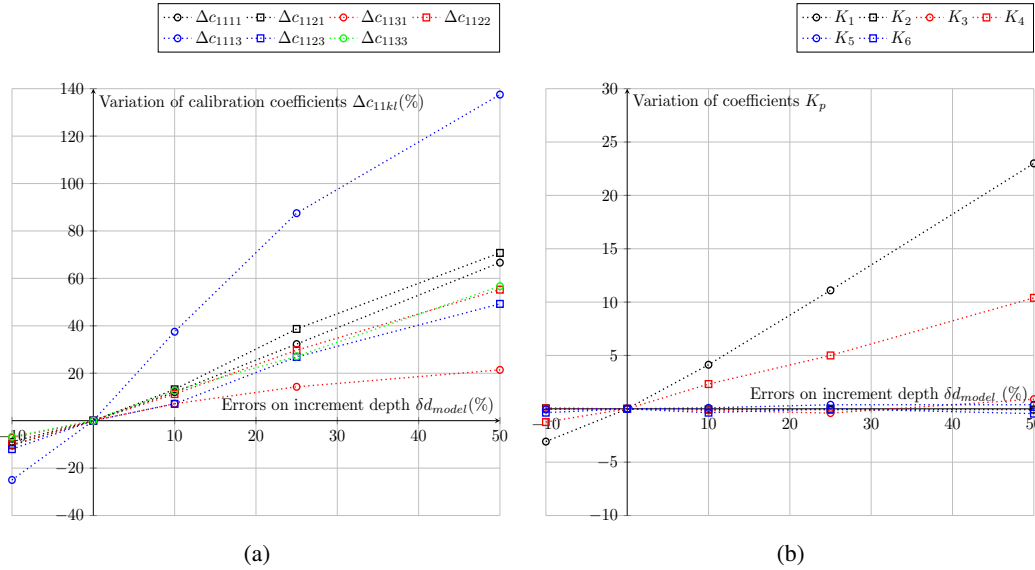


Figure 7: Variation of the calibration coefficients c_{11kl} (a) and the coefficients K_p (b) for different errors on increment depth δd_{model} ranging from -10% to 50% of the desired increment depth d_{model}

tion of coefficients K_p , $1 \leq p \leq 6$ (Eq.18-20). K_1 and K_4 which appear respectively in the expression of $\delta\sigma_x$ and $\delta\sigma_y$ are the most sensitive to errors on increments depth.

The same study is done at the $0/90$ interface which correspond to four increments. The variations of the coefficients c_{ijkl} are presented in Fig. 8a and those of coefficients K_p , $1 \leq p \leq 6$ are presented in Fig 8b. It can be seen that there are coefficients whose variations present a change of slope at the interface and those whose variations are linear. The coefficients c_{4411} , c_{4421} and c_{4431} , which are calculated from the first load case (longitudinal uni-axial tensile stress, Eq.6), vary linearly. This is due to the fact that one goes from a 0 -degree oriented layer with a higher longitudinal Young's modulus to a 90 -degree oriented layer with a lower longitudinal Young's modulus, there is therefore no sudden variation in relaxation deformations at the beginning of the transition. In the contrary, for coefficients c_{4413} , c_{4423} and c_{4433} , which are calculated from load case 2 (transverse uni-axial tensile stress, Eq.7), as soon as the layer oriented at 90 degrees is drilled, there is a non-linear change of the Young's modulus in the transverse direction. Similarly, there is a non-linear increase in the shear modulus at the $0/90$ interface, this is the reason why the variation of the coefficient c_{4422} presents a change of slope.

For composite laminates, it is difficult to model precisely the location of the different ply-ply interfaces because of the uncertainties on the layers' thickness. Generally, the mean thickness of the layers are considered in finite element simulations, however this can cause mismatches between the simulation and the experimentation of the hole drilling process and cause deviations on the calibration coefficients similar to those presented on Fig. 8a and 8b. For example, due to the uncertainties on the layers' thickness, one can go from a layer to the next in the experimentation without reaching the interface in the simulation or vice versa. To avoid such errors, the real thickness of each layer must be considered in the numerical simulation, unfortunately, such information can only be accessed precisely by cutting and observing the sample at the hole location.

4.3. Angular deviation of the gages from their theoretical position

In Eq. 5, coefficients c_{12} and c_{32} are always equal to zero if the gage 1 is oriented in on-axis direction of the first layer. But, if there is an angular offset when gluing the gages (Fig. 5b), the calibration coefficients vary. c_{12} and c_{32} are no longer equal to zero. Not taking these variations into account in the calculations leads to errors on residual stresses determination.

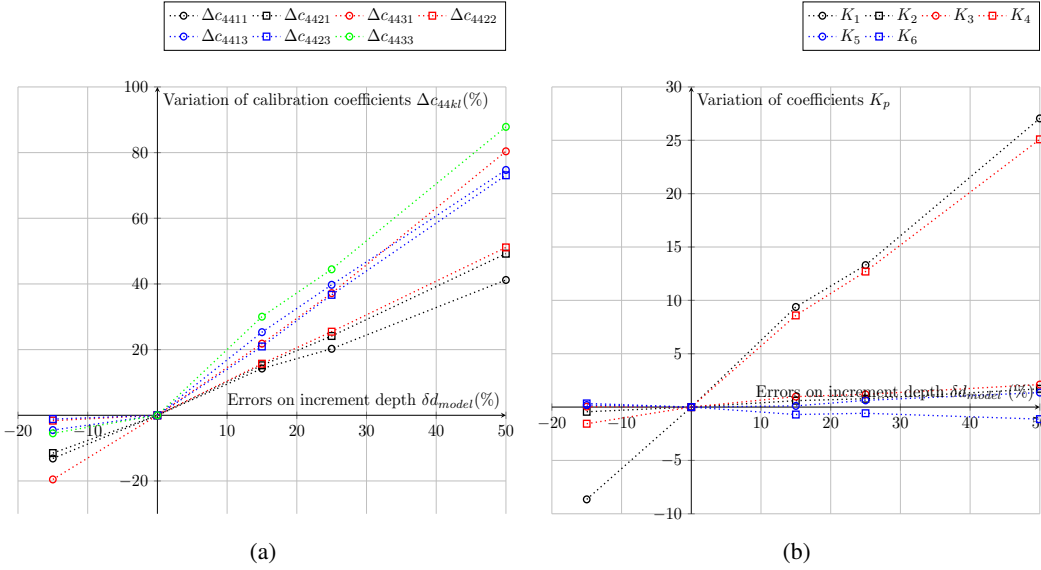


Figure 8: Variation of the calibration coefficients c_{44kl} (a) and the coefficients K_p (b) for different errors on increment depth δd_{model} ranging from -15% to 50% of the desired increment depth d_{model} at the $0/90$ interface

Table 3

variation of the calibration coefficients c_{11kl} for different angular deviations in the counter-clockwise direction

Angular deviation	c_{1111}	c_{1121}	c_{1131}	c_{1112}	c_{1122}	c_{1132}	c_{1113}	c_{1123}	c_{1133}
0 degrees	-0.0291	-0.0106	-0.0014	0.0000	-0.0713	0.0000	0.0008	-0.0268	-0.0545
2 degrees	-0.0292	-0.0092	-0.0014	-0.0024	-0.0696	0.0020	0.0007	-0.0287	-0.0548
5 degrees	-0.0296	-0.0070	-0.0014	-0.0064	-0.0655	0.0061	0.0004	-0.0321	-0.0556
10 degrees	-0.0301	-0.0040	-0.0016	-0.0153	-0.0557	0.0122	-0.0004	-0.0361	-0.0549

Different angular deviations, in the counter-clockwise direction, are introduced in the numerical model to study variations of calibration coefficients (Table 3).

Here, Eq. 15, 16 and 17 become:

$$\sigma_x^i = (k_8 \epsilon_1^i + k_9 \epsilon_2^i + k_{10} \epsilon_3^i) \sqrt{E_x E_y} \quad (21)$$

$$\sigma_y^i = (k_{11} \epsilon_1^i + k_{12} \epsilon_2^i + k_{13} \epsilon_3^i) \sqrt{E_x E_y} \quad (22)$$

$$\sigma_{xy}^i = (k_{14} \epsilon_1^i + k_{15} \epsilon_2^i + k_{16} \epsilon_3^i) \sqrt{E_x E_y} \quad (23)$$

And, Eq. 18, 19 and 20 become:

$$\delta \sigma_x^i = (K_7 \epsilon_1^i + K_8 \epsilon_2^i + K_9 \epsilon_3^i) \sqrt{E_x E_y} \quad (24)$$

$$\delta \sigma_y^i = (K_{10} \epsilon_1^i + K_{11} \epsilon_2^i + K_{12} \epsilon_3^i) \sqrt{E_x E_y} \quad (25)$$

$$\delta \sigma_{xy}^i = (K_{13} \epsilon_1^i + K_{14} \epsilon_2^i + K_{15} \epsilon_3^i) \sqrt{E_x E_y} \quad (26)$$

The analysis of the radial strain field shows that, for an angular shift of 0-10 degrees, the absolute values of ϵ_1^i (gage 1) increase, those of ϵ_2^i (gage 2) decrease and those of ϵ_3^i (gage3) are almost constant for load case 1, 3 and 2 respec-

tively (Eq. 6-8). Consequently, the absolute values of the coefficient c_{11} increase, those of the coefficient c_{22} decrease and those of c_{33} vary very lightly (table 3 ref). However, this variation is not monotonous and is reversed with larger angles since the distribution of the radial strain around the hole is globally sinusoidal. c_{13} is small in terms of value, but is the most sensitive to angular deviations (Fig. 9a). The variation of coefficients c_{21} , c_{22} , c_{23} , depends on the deviation direction.

The influence of the angular deviations on residual stresses calculation can be observed by the variation of coefficients K_p , $7 \leq p \leq 15$ (Fig. 9b) of Eq. 24-26. K_8 is particularly sensitive to this error. The angular deviation of the gages is a frequent error because of the difficulty to locally orient the gage 1 of the rosette in the direction of the fibers. However, as shown in this section, an accurate calculation of residual stress uncertainties needs a rigorous control of the angular offset of the gages.

4.4. Hole eccentricity errors

Centering the spindle, in relation to the hole, is a delicate operation that must be performed with great care. Any eccentricity e_c , α_c (Fig. 5c) of the hole leads to errors in the values of the calibration coefficients.

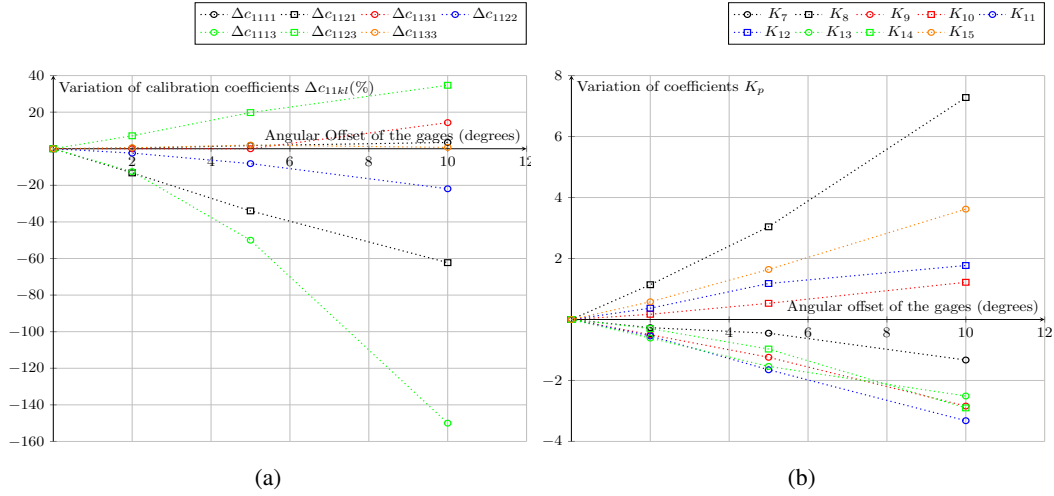


Figure 9: Variation of the calibration coefficients c_{11kl} (a) and the coefficients K_p (b) for different angular deviations of the gages from their ideal position ranging from 0 to 10 degrees in the counter-clockwise direction

Table 4

variation of the calibration coefficients c_{11kl} for different radial eccentricities of the hole along x-axis

e_c/r_m	c_{1111}	c_{1121}	c_{1131}	c_{1122}	c_{1113}	c_{1123}	c_{1133}
0	-0.0291	-0.0106	-0.0014	-0.0713	0.0008	-0.0268	-0.0545
-2%	-0.0268	-0.0138	-0.0015	-0.0782	-0.0003	-0.0258	-0.0546
-5%	-0.0232	-0.0190	-0.0018	-0.0891	-0.0021	-0.0247	-0.0565
-10%	-0.0175	-0.0283	-0.0026	-0.1059	-0.0054	-0.0225	-0.0526
2%	-0.0315	-0.0074	-0.0015	-0.0643	0.0019	-0.0274	-0.0559
5%	-0.0356	-0.0032	-0.0018	-0.0529	0.0034	-0.0277	-0.0542
10%	-0.0424	0.0031	-0.0025	-0.0359	0.0061	-0.0303	-0.0519

The study of hole eccentricity errors on calibration coefficients is decoupled into a study of the influence of radial eccentricity (Table 4) and a study of the influence of angular eccentricity (Table 5). The variations of coefficients K_p are presented in Fig. 10b and 10d.

Influence of radial eccentricity: $\alpha_c = 0$ and e_c varies along x-axis

The coefficients vary linearly with radial eccentricity (Fig. 10a). The absolute values of coefficients c_{1111} and c_{1113} (which are calculated from the strain of gage 1) increase with positive values of e_c and decrease with negative values of e_c . This is explained by the fact that the closer the hole is to the gage 1, the greater the strains measured by this gage whether the load is in the longitudinal or transverse (Poisson effect) direction. The strain measured from the partition corresponding to gage 3 is similar for positive and negative values of e_c , thus, the variations of the coefficients calculated from this gage, i.e. c_{1131} and c_{1133} , are symmetrical with respect to the y axis.

The variation of coefficients K_p , $1 \leq p \leq 6$, depends on the chosen radial direction. Here, only the results along the x-axis are presented. The coefficients K_1 and K_5 in the expression of $\delta\sigma_x$ and $\delta\sigma_{xy}$ are the most sensitive to the radial eccentricity along x-axis (Fig. 10b).

Influence of angular eccentricity: $e_c/r_m = 5\%$ and α_c varies in the counter-clockwise direction

The radial eccentricity is fixed to 5% of r_m (i.e. 0.12 mm here) and the angular eccentricity is varied from 0 to 10 degrees in the counter-clockwise direction. The coefficient c_{31} is the most sensitive to the angular eccentricities (Fig. 10c). In fact, the larger the angular eccentricity, the closer the hole is to the gage 3 and the greater the Poisson effect for load case 1. Coefficients K_{11} , K_{14} and K_{12} have a relatively large deviation between $\alpha_c = 0$ degrees and $\alpha_c = 2$ degrees. However, between $\alpha_c = 2$ degrees and $\alpha_c = 10$ degrees, the coefficients K_p vary little (Fig. 10d). It is important to note the appearance of two non-null coefficients in the matrix $[c_{kl}]$. If $\alpha_c \neq 0$, $c_{12} \neq 0$ and $c_{32} \neq 0$, except for small angles ($\alpha_c \leq 2$ degrees) for which $c_{12} \approx 0$ (Table 5).

Like the errors studied previously, hole eccentricity errors can be minimized but not be avoided. Given the deviations generated on the coefficients K_p , one cannot calculate the residual stresses accurately without taking into account the experimental errors. A precise measurement of these errors makes it possible to calculate the uncertainties on the residual stresses or even to correct their effects.

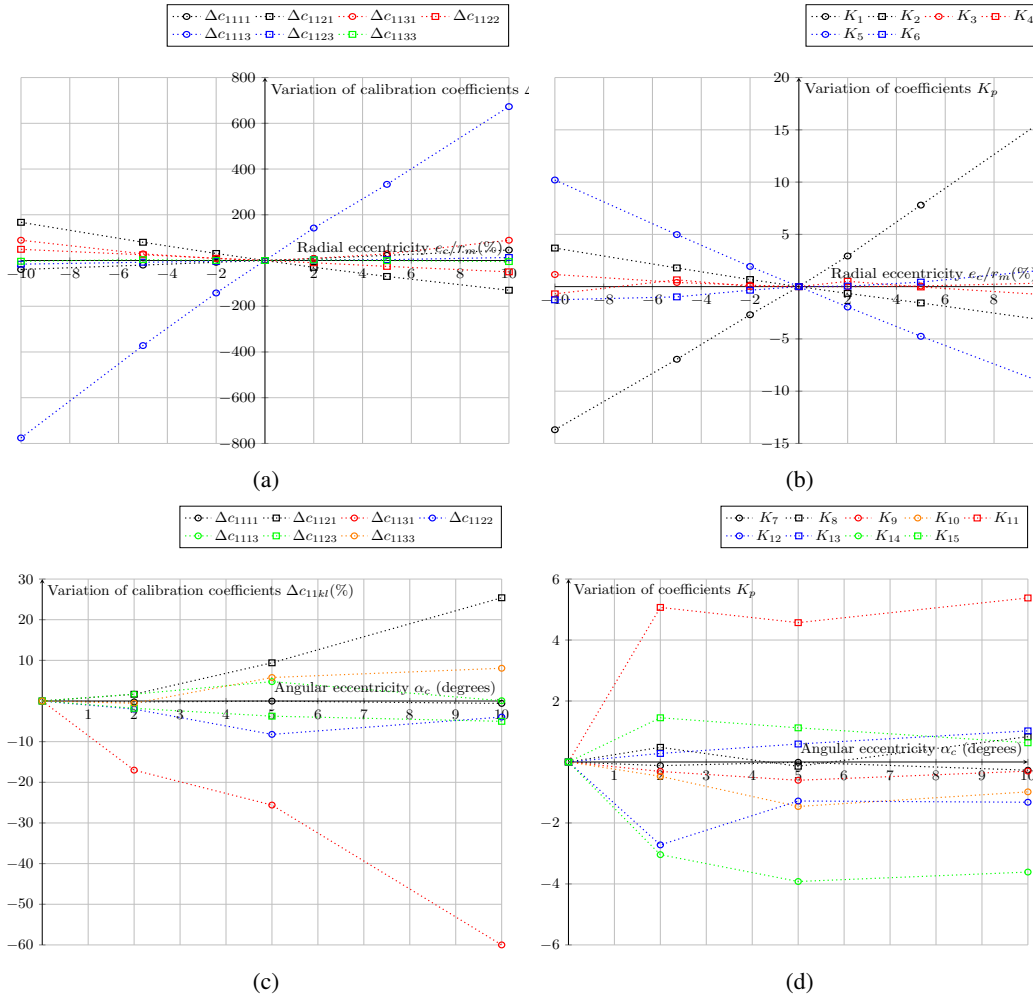


Figure 10: Variation of the calibration coefficients c_{11kl} (a) and the coefficients K_p (b) for different radial eccentricities of the hole along x-axis, Variation of the calibration coefficients c_{11kl} (c) and the coefficients K_p (d) for a radial eccentricity fixed to 5% of the mean radius ($e_c/r_m = 5\%$) and for different angular eccentricities varying from 0 to 10 degrees in the counter-clockwise direction

Table 5

variation of the calibration coefficients c_{11kl} for a radial eccentricity fixed to 5% of the mean radius ($e_c/r_m = 5\%$) and for different angular eccentricities varying from 0 to 10 degrees in the counter-clockwise direction

α_c	c_{1111}	c_{1121}	c_{1131}	c_{1112}	c_{1122}	c_{1132}	c_{1113}	c_{1123}	c_{1133}
0 degrees	-0.0356	-0.0032	-0.0018	0.0000	-0.0529	0.0000	0.0034	-0.0277	-0.0542
2 degrees	-0.0355	-0.0032	-0.0015	0.0000	-0.0519	-0.0146	0.0035	-0.0272	-0.0539
5 degrees	-0.0356	-0.0035	-0.0013	0.0011	-0.0486	-0.0131	0.0036	-0.0267	-0.0574
10 degrees	-0.0354	-0.0040	-0.0007	-0.0006	-0.0508	-0.0155	0.0034	-0.0263	-0.0586

5. Numerical correction of the calibration coefficients for composite laminates

The experimental errors can be minimized by optimizing the used experimental device but they cannot be avoided (Scenario 2 of section 4). One solution is to propose a method to correct the effect of these errors on the results. Some researchers have shown that residual stresses can be reliably calculated from relaxation strains measured with category 2 errors [16, 32, 33, 15]. For this, the calibration coefficients

must be adequately corrected. For thin isotropic materials, for which residual stresses are considered uniform in thickness, Ajovalasit [16] proposed the theory of eccentric-hole method. This theory consists in correcting the calibration coefficients by introducing the eccentricity of the hole in the equations. Finite element simulations was used by Blödorn et al. [33] to correct the effect of hole bottom chamfer and by Barsanti et al. [32] to correct eccentricity of the hole but they limited their work to isotropic materials.

In this work, a numerical approach is proposed which consists in taking into account experimental errors in the numerical model to correct the calibration coefficients (Fig. 11). This allow to remove the mismatches between the numerical simulation and the experimental process (Scenario 3 of section 4). The correction method requires a numerical model that has the flexibility to take into account different category 2 errors, hence the interest of developing a configurable model (section 4.1, Fig. 6) . However, this numerical-experimental coupling requires an accurate experimental measurement of the considered error. Consider a reference test for which the parameters have been optimized to minimize errors (Eq. 27), a test with at least one category 2 error introduced (Eq. 28) and the corrected residual stresses (Eq. 29).

$$\{\sigma_l^i\}_{ref} = [C_{ii}]_{ref}^{-1} \{\epsilon_k^i\}'_{ref} \quad (27)$$

$$\{\sigma_l^i\}_{error} = [C_{ii}]_{ref}^{-1} \{\epsilon_k^i\}'_{error} \quad (28)$$

$$\{\sigma_l^i\}_{corr} = [C_{ii}]_{corr}^{-1} \{\epsilon_k^i\}'_{error} \quad (29)$$

$$1 \leq l \leq 3, 1 \leq k \leq 3$$

Where $\{\sigma_l^i\}_{ref}$, $\{\sigma_l^i\}_{error}$ and $\{\sigma_l^i\}_{corr}$ are respectively the reference residual stresses, the residual stresses calculated with the error and the corrected residual stresses of increment i.

$[C_{ii}]_{ref}^{-1}$ and $[C_{ii}]_{corr}^{-1}$ are respectively the inverse of the matrix of the initial and corrected calibration coefficients of increment ij (j=i).

$\{\epsilon_k^i\}'_{ref}$ and $\{\epsilon_k^i\}'_{error}$ are respectively the reference relaxation strains and the relaxation strain measured with the error for increments i exclusively. The relaxation strains exclusively due to increment i are the subtraction of the total strains measured at the surface ($\{\epsilon_k^i\}$) and the strains due to the previous increments : $\{\epsilon_k^i\}' = \{\epsilon_k^i\} - \sum_{j=1}^{i-1} [C_{ij}] \{\sigma_l^j\}$.

The correction must be made in such a way as to obtain ideally $\{\sigma_l^i\}_{corr} = \{\sigma_l^i\}_{ref}$.

$$\{\sigma_l^i\}_{corr} = \{\sigma_l^i\}_{ref} \Rightarrow [C_{ii}]_{corr}^{-1} \{\epsilon_k^i\}'_{error} = [C_{ii}]_{ref}^{-1} \{\epsilon_k^i\}'_{ref} \quad (30)$$

The expansion of Eq. 30, for a considered increment, gives a system of three equations which are satisfied by considering a term by term equality for each equation. Thus, the inverse of the matrix of the corrected calibration coefficients is given by Eq. 31.

$$[C_{ii}]_{corr}^{-1} = [C_{ii}]_{ref}^{-1} [S_{ii}] \quad (31)$$

Where $[S_{ii}]$ is the correction matrix:

$$[S_{ii}] = \begin{bmatrix} \frac{\epsilon_1^i}{\epsilon_{1(err)}^i} & 0 & 0 \\ 0 & \frac{\epsilon_2^i}{\epsilon_{2(err)}^i} & 0 \\ 0 & 0 & \frac{\epsilon_3^i}{\epsilon_{3(err)}^i} \end{bmatrix} \quad (32)$$

Experimentally, only the relaxation strains for the real parameters $\epsilon_{k(err)}^i$ are known (Scenario 2 of section 4). Therefore, the correction is based on a numerical estimation of the matrix $[S_{ii}]$. For the first increment, the corrected calibration coefficients can be written from Eq. 31:

$$C_{11kl}(corr) = C_{11kl}(ref) \frac{\epsilon_{k(err)}^1}{\epsilon_k^1} \quad (33)$$

From Eq. 6-8, one can write:

$$C_{11kl}(ref) = \frac{\epsilon_k^1}{\sigma_0} \quad (34)$$

Where σ_0 is the magnitude of the load cases.

Then, Eq. 33 becomes:

$$C_{11kl}(corr) = \frac{\epsilon_{k(err)}^1}{\sigma_0} \quad (35)$$

By comparing Eq. 35 to Eq. 6-8, one understands that, for the first increment, the numerical correction simply consists in recalculating the calibration coefficient with the conventional method (Eq. 6-8) by taking into account the errors of interest in the simulation.

Application 2: numerical validation of the correction method

In this application, the incremental hole drilling method is numerically simulated with a hole eccentricity of 10% of r_m (i.e. 0.257 mm). The obtained numerical residual stresses are corrected using the method described in section 5 and compared to the reference residual stresses (simulation without eccentricity). The results are presented in Table 6. The same stress profile is applied to the 2 simulations as initial state of residual stresses (input). The same material and gages geometry as application 1 (Section 3) are used.

The results presented in Table 6 show that residual stresses calculated numerically with a hole eccentricity of 10% of r_m can be corrected by determining the appropriate $[S_{ii}]$ matrix. All the data used to calculate the results presented in Table 6 are given in the appendix B. Results with other category 2 errors, other initial stress profiles and the $[S_{ii}]$ matrices used

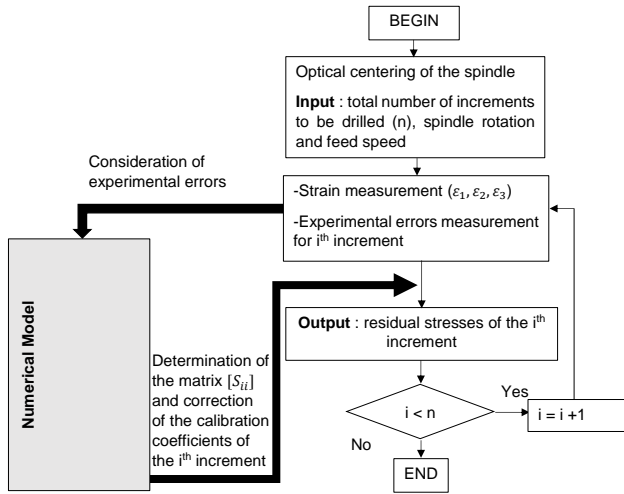


Figure 11: Numerical correction of the calibration coefficients by a configurable experimental-numerical coupling

are also given in the appendix. As expected, the corrected values are equal to the reference values. This is explained by the fact that the reference values and those with errors are known which allows to calculate the exact $[S_{ii}]$ matrices. Experimentally, the reference values are not known, the correction is therefore based on a numerical estimation of the real $[S_{ii}]$ matrices. Here, the results only validate the mathematical approach of the proposed method. Qualitative and quantitative experimental testing data are needed to experimentally validate the method.

6. Conclusion

In this work, the influence of three main experimental errors on the accuracy of the incremental hole drilling method, for a $[0_2/90_2]_s$ carbon/epoxy composite laminates, is numerically investigated. These errors are the errors on increment depth, the angular deviation of the gages from their theoretical position and the eccentricity of the hole with respect to the strain-gage rosette. A precise determination of the calibration coefficients is crucial to ensure the reliability of the residual stresses. A detailed analysis of the sensitivity of the calibration coefficients to the studied errors is presented. This paper introduces a novel approach based on a configurable numerical-experimental coupling to correct the calibration coefficients for composite laminates.

The analysis of the sensitivity of the calibration coefficients showed that they are very sensitive to experimental errors, particularly radial eccentricity of the hole. A radial eccentricity equal to 10% of the mean radius of the gages (i.e. 0.257 mm for EA-06-062RE-120 strain gages) along the x-axis causes 130% error on the coefficient c_{1121} and up to 673% error on c_{1113} . The matrix diagonal coefficients, c_{11kk} , $k = l$, are more sensitive to errors on increment depth. The angular deviation of the gages from their theoretical position is one of the most frequent error. However, the coeffi-

Table 6

Numerical validation of the proposed correction method: comparison between the reference residual stresses, the corrected residual stresses and residual stresses with an eccentric hole obtained by numerical simulations of the incremental hole drilling for the considered initial residual stress profile.

Residual stresses	Reference (MPa)	Eccentric hole, 10% of r_m (MPa)	Corrected (MPa)
σ_x^1	-5.79	-7.93	-5.79
σ_{xy}^1	0.35	1.23	0.35
σ_y^1	-3.28	-3.06	-3.28
σ_x^2	-223.50	-276.71	-223.50
σ_{xy}^2	14.11	52.96	14.11
σ_y^2	-38.76	-34.90	-38.76
σ_x^3	-1372.29	-1478.10	-1372.29
σ_{xy}^3	62.68	258.19	62.68
σ_y^3	-227.58	-220.03	-227.58
σ_x^4	28.66	181.57	28.66
σ_{xy}^4	15.07	-40.18	15.07
σ_y^4	-72.10	-62.45	-72.10
σ_x^5	-300.24	-239.31	-300.24
σ_{xy}^5	-19.91	7.17	-19.91
σ_y^5	-359.27	-353.64	-359.27
σ_x^6	533.35	639.62	533.35
σ_{xy}^6	-115.81	-232.50	-115.81
σ_y^6	-739.31	-693.20	-739.31

icients K_p , $7 \leq p \leq 15$ which are in the expression of residual stress errors ($\delta\sigma_i^l$) are less sensitive to this error.

The calibration coefficients can be corrected by calculating the matrix $[S_{ii}]$ which is given by the ratios of the reference relaxation strains (optimized experimental parameters) and the relaxation strains measured with errors. However, in practice, if a correction is needed, then only the relaxation strains measured with errors are available. Thus, the matrix $[S_{ii}]$ must be approximated by numerical simulations. For this, precise measurements of the experimental errors is required. The proposed correction method (its mathematical approach) is numerically validated by numerical simulations of the incremental hole drilling method. However, further work is needed to validate the method experimentally with qualitative testing data.

By contributing to improve the calibration coefficients calculation accuracy, this work contributes to determine residual stresses more reliably in composite laminates. This will permit to estimate more precisely the mechanical properties of such materials and therefore, to better adapt their functionalities.

Declaration of Competing Interest

The authors declare that they have no known competing financial interests or personal relationships that could have appeared to influence the work reported in this paper.

References

- [1] Ulrike G. K. Wegst, Hao Bai, Eduardo Saiz, Antoni P. Tomsia, and Robert O. Ritchie. Bioinspired structural materials. *Nature Materials*, 14(1):23–36, January 2015. Number: 1 Publisher: Nature Publishing Group.
- [2] Patricia P Parlevliet, Harald EN Bersee, and Adriaan Beukers. Residual stresses in thermoplastic composites—a study of the literature—part i: Formation of residual stresses. *Composites Part A: Applied Science and Manufacturing*, 37(11):1847–1857, 2006.
- [3] Nahed Ahmed Abdel-Raheem, Sawsan Fakhry Halim, and Ahmed Hatem Al-Khoribi. The effect of different curing conditions on hardness, thickness, and residual stress of carbon fiber reinforced epoxy composites. *Journal of Composite Materials*, 52(14):1959–1970, June 2018.
- [4] Nuri Ersoy and Oktem Vardar. Measurement of residual stresses in layered composites by compliance method. *Journal of Composite Materials*, 34(7):575–598, 2000.
- [5] Jan-Anders E. Manson and James C. Seferis. Process Simulated Laminate (PSL) : A Methodology to Internal Stress Characterization in Advanced Composite Materials. *Journal of Composite Materials*, 26(3):405–431, March 1992. Publisher: SAGE Publications Ltd STM.
- [6] J A Barnes. THE FORMATION OF RESIDUAL STRESSES IN LAMINATED THERMOPLASTIC COMPOSITES. page 16, 1994.
- [7] Patricia P. Parlevliet, Harald E. N. Bersee, and Adriaan Beukers. Residual stresses in thermoplastic composites – a study of the literature. Part III: Effects of thermal residual stresses. *Composites Part A: Applied Science and Manufacturing*, 38(6):1581–1596, June 2007.
- [8] KS Kim and HT Hahn. Residual stress development during processing of graphite/epoxy composites. *Composites Science and Technology*, 36(2):121–132, 1989.
- [9] Michael W Hyer. Some observations on the cured shape of thin unsymmetric laminates. *Journal of Composite Materials*, 15(2):175–194, 1981.
- [10] Paul Predecki and Charles S Barrett. Stress measurement in graphite/epoxy composites by x-ray diffraction from fillers. *Journal of composite materials*, 13(1):61–71, 1979.
- [11] MPIM Eupe and PC Powell. A modified layer removal analysis for the determination of internal stresses in polymer composites. *Journal of thermoplastic composite materials*, 10(4):334–352, 1997.
- [12] GS Schajer. Measurement of non-uniform residual stresses using the hole-drilling method. part i—stress calculation procedures. *Journal of Engineering Materials and Technology*, 1988.
- [13] Jiang Guo, Haiyang Fu, Bo Pan, and Renke Kang. Recent progress of residual stress measurement methods: A review. *Chinese Journal of Aeronautics*, November 2019.
- [14] ASTM. Astm e837-01e1, standard test method for determining residual stresses by the hole-drilling strain-gage method, astm international, west conshohocken, pa, 2001, www.astm.org. 2001.
- [15] GS Schajer and E Altus. Stress calculation error analysis for incremental hole-drilling residual stress measurements. *Journal of Engineering Materials and Technology*, 1996.
- [16] A Ajovalasit. Measurement of residual stresses by the hole-drilling method: influence of hole eccentricity. *The journal of strain analysis for engineering design*, 14(4):171–178, 1979.
- [17] M. Beghini, L. Bertini, and L. F. Mori. Evaluating Non-Uniform Residual Stress by the Hole-Drilling Method With Concentric and Eccentric Holes. Part II: Application of the Influence Functions to the Inverse Problem. *Strain*, 46(4):337–346, 2010. _eprint: <https://onlinelibrary.wiley.com/doi/pdf/10.1111/j.1475-1305.2009.00684.x>.
- [18] M. Beghini, L. Bertini, and L. F. Mori. Evaluating Non-Uniform Residual Stress by the Hole-Drilling Method with Concentric and Eccentric Holes. Part I. Definition and Validation of the Influence Functions. *Strain*, 46(4):324–336, 2010. _eprint: <https://onlinelibrary.wiley.com/doi/pdf/10.1111/j.1475-1305.2009.00683.x>.
- [19] Josef Mathar. Determination of inherent stresses by measuring deformations of drilled holes. 1933.
- [20] W. Soete and R. Vancrombrugge. An industrial method for the determination of residual stresses. *Proc. SESA*, 8(1):17–28, 1950.
- [21] N. J. Rendler and I. Vigness. Hole-drilling strain-gage method of measuring residual stresses. *Experimental Mechanics*, 6(12):577–586, December 1966.
- [22] Charles W. Bert and Gary L. Thompson. A Method for Measuring Planar Residual Stresses in Rectangularly Orthotropic Materials. *Journal of Composite Materials*, 2(2):244–253, April 1968.
- [23] M. Bijak-Zochowski. A semidestructive method of measuring residual stresses. In (*Verein Deutscher Ingenieure, Internationale Konferenz ueber experimentelle Spannungsanalyse, 6 th, Munich, West Germany, Sept. 18-22, 1978.*) *VDI-Berichte.*, pages 469–476, 1978.
- [24] G. S. Schajer. Application of Finite Element Calculations to Residual Stress Measurements. *Journal of Engineering Materials and Technology*, 103(2):157–163, April 1981.
- [25] A. Niku-Lari, J. Lu, and J. F. Flavenot. Measurement of residual-stress distribution by the incremental hole-drilling method. *Journal of Mechanical Working Technology*, 11(2):167–188, May 1985.
- [26] M. T. Flaman and B. H. Manning. Determination of residual-stress variation with depth by the hole-drilling method. *Experimental Mechanics*, 25(3):205–207, September 1985.
- [27] G. S. Schajer and L. Yang. Residual-stress measurement in orthotropic materials using the hole-drilling method. *Experimental Mechanics*, 34(4):324–333, December 1994.
- [28] Jong-Ning Aoh and Chung-Sheng Wei. On the Improvement of Calibration Coefficients for Hole-Drilling Integral Method: Part I—Analysis of Calibration Coefficients Obtained by a 3-D FEM Model. *Journal of Engineering Materials and Technology*, 124(2):250–258, April 2002.
- [29] O. Sicot, X. L. Gong, A. Cherouat, and J. Lu. Determination of Residual Stress in Composite Laminates Using the Incremental Hole-Drilling Method. *Journal of Composite Materials*, 37(9):831–844, May 2003.
- [30] Mahmood M. Shokrieh and Ahmad R. Ghasemi K. Simulation of Central Hole Drilling Process for Measurement of Residual Stresses in Isotropic, Orthotropic, and Laminated Composite Plates. *Journal of Composite Materials*, 41(4):435–452, February 2007.
- [31] A. R. Ghasemi and M. M. Mohammadi. Residual stress measurement of fiber metal laminates using incremental hole-drilling technique in consideration of the integral method. *International Journal of Mechanical Sciences*, 114:246–256, August 2016.
- [32] Michele Barsanti, Marco Beghini, Leonardo Bertini, Bernardo D Monelli, and Ciro Santus. First-order correction to counter the effect of eccentricity on the hole-drilling integral method with strain-gage rosettes , First-order correction to counter the effect of eccentricity on the hole-drilling integral method with strain-gage rosettes. *The Journal of Strain Analysis for Engineering Design*, 51(6):431–443, August 2016. Publisher: IMECHE.
- [33] Rodrigo Blödorn, Lucas Bonomo, Matias Viotti, Rolf Schroeter, and Albertazzi Jr. Calibration Coefficients Determination Through Fem Simulations for the Hole-Drilling Method Considering the Real Hole Geometry. *Experimental Techniques*, 41, September 2016.
- [34] G. S. Schajer. Compact Calibration Data for Hole-Drilling Residual Stress Measurements in Finite-Thickness Specimens. *Experimental Mechanics*, February 2020.
- [35] S. Akbari, F. Taheri-Behrooz, and M. M. Shokrieh. Characterization of residual stresses in a thin-walled filament wound carbon/epoxy ring using incremental hole drilling method. *Composites Science and Technology*, 94:8–15, April 2014.
- [36] Paulius Ragauskas and Rimantas Belevičius. Identification of material properties of composite materials. *Aviation*, 13(4):109–115, De-

